4-22-2021

From Molecules to Mountains: A Multi-Proxy Investigation into Ancient Climate and Topography of the Pacific Northwest, USA

Alex McLean
Portland State University

From Molecules to Mountains:

A Multi-Proxy Investigation into Ancient Climate and

Topography of the Pacific Northwest, USA

by

Alex McLean

A thesis submitted in partial fulfillment of the
requirements for the degree of

Master of Science
in
Geology

Thesis Committee:
John Bershaw, Chair
Martin Streck
Scott Burns

Portland State University
2021

ABSTRACT

The modern Cascades are a north-south striking mountain range that intercepts Pacific Ocean-derived moisture resulting in orographic precipitation on the western flank and a relatively arid rain shadow in the lee. Because of the strong coupling between topography and climate and consistent moisture source (Pacific Ocean) throughout the year, the region is ideally situated for paleoclimate studies that utilize the isotopic composition ($\delta^{18}O$ and δD) of meteoric water to determine when uplifts occurred. Here, I synthesize the spatial and temporal evolution of stable isotopes in paleowater proxies across the Pacific Northwest during the Cenozoic. New volcanic glass (δD) and paleosol carbonate stable isotope ($\delta^{18}O$) results from central Oregon are presented, along with published proxy data, including fossil teeth, smectites, and carbonate concretions. I interpret a polygenetic history of Cascade Mountain topographic uplift along-strike, characterized by: 1) Steady uplift of the Washington Cascades through the Cenozoic due long-term arc rotation and shortening against a Canadian buttress, and 2) Uplift of the Oregon Cascades to similar-to-modern elevations by the late Oligocene, followed by topographic stagnation as extension developed into the Neogene. Since the Miocene, meteoric water $\delta^{18}O$ values have decreased in Oregon, possibly due to emergence of the Coast Range and westward migration of the coastline. Estimates of ancient deuterium excess (d-excess) based on multiple, independent proxies suggest a trend of aridification in central Oregon during this time. Spatial variability in isotopic change across the Pacific Northwest suggests that secular global climate change is not the primary forcing

mechanism behind isotopic trends, though Milankovitch cycles may be partly responsible for relatively short-term variation in isotopic results.

Acknowledgements

I could probably write an entire second thesis on all the help I received along the way, but a page will have to suffice. I'd like to thank Dr. John Bershaw, my adviser on this quest, for the wisdom, patience, revisions, music recommendations, and friendship. If I had a hop for each time John corrected me when I thought up was up, when in fact it is down, I'd be able to brew a lifetime supply of drinks. I'd like to thank my committee members, Dr. Scott Burns and Dr. Martin Streck, for their valuable assistance in all sorts of odd corners of research.

I'd like to extend a deep thanks to my parents and my brother, whose decades of support provide the foundation of my success in all walks of life. To my loving partner, Matt, for believing in me every second of the past two and half years, for the patience, the rides, the lunches, and more. To my peers in the department: particularly my research group mates, Jane and Cameron, for their comradery and insight; to Bryce for walking me through the basics of coding; to Cassandra and Ryan for being such great friends; and to all others who I can't fit here.

Finally, I'd like to thank the Graduate Employees' Union of Portland State University, for all we have been able to accomplish for workers now and workers yet to come.

And, of course, to my cat, Giskard, for being my pal.

TABLE OF CONTENTS

List of Tables

LIST OF FIGURES

1.0 Introduction

Stable isotope ratios of water can illuminate temporal changes in a region's climate and topography (Rowley and Garzione, 2007; Quade et al., 2007; Savin, 1982). Deuterium-hydrogen ratios in hydrated volcanic glass (δ^2H) and oxygen isotope ratios in pedogenic carbonates ($\delta^{18}O$) have been widely utilized to constrain paleoclimate (Cerling and Quade, 1993; Garizone et al., 2000; Cassel and Breecker, 2017; Saylor and Horton, 2014). While studies have looked at Cascade Mountain uplift using one of these tools (e.g. Kohn and Law, 2006; Kohn et al., 2002; Bershaw et al., 2019; Takeuchi and Larson, 2005; Takeuchi et al., 2010), few studies have taken a multi-proxy approach.

Combining stable isotope data from multiple, independent proxies can reduce uncertainty by better constraining forcing mechanisms of isotopic change (Currie et al., 2016; Mulch and Chamberlain, 2007). I present new soil carbonate $\delta^{18}O$ and volcanic glass δD data, in addition to a synthesis of published proxy data that spans the Cenozoic across the Pacific Northwest, to better understand the region's climatic and topographic development.

In my discussion, I start by assessing which data likely reflects ancient meteoric water, followed by an interpretation of spatial (Pacific Northwest) and temporal (Cenozoic) patterns in topography and climate. I compare temporal patterns of isotopic variation to the record of global Cenozoic $\delta^{18}O$ change and Milankovitch-scale variation (Zachos et al., 2001) to investigate the influence of global climate on isotopic patterns. Lastly, I reconstruct ancient deuterium-excess (d-excess) to explore the coupling of climate and topography through the Neogene.

2.0 Background

2.1 Modern Climate of the Pacific Northwest

The Pacific Northwest is situated in the mid-latitudes of the northern hemisphere with a climate that is classified as Mediterranean, with cool, wet winters and warm, dry summers. Orographic precipitation is significant in mountains across the region, including the Cascade Volcanic Arc (Cascades), the Olympic Mountains in Washington, and the Oregon Coast Range. The Cascades create a significant rainshadow in the lee (east) side of the range, exemplified by Sandy, Oregon (windward) receiving 210cm/year of precipitation, compared to Maupin, Oregon receiving 30cm/year in the lee, despite only being separated by ~115 km (World Climate Atlas, 2020). Modern westerly air-flow patterns are interpreted to have remained relatively constant since the Cenozoic based on depositional patterns of wind-blown ash (Robinson et al., 1990).

2.2 Regional Geologic and Topographic History

In Oregon and Washington, the Cascades extend north-south from British Columbia, Canada, to California, USA. The Cascades are a magmatic arc that formed from the subduction of the Juan de Fuca Plate under the North American Plate (Priest, 1990). The onset of Cascade volcanism is interpreted to have begun ~45 Ma, approximately 5 Ma after the accretion of the Siletzia Terrane (Wells et. al, 2013). By ~35 Ma, the entire magmatic arc had been established from northern California to Mt. Rainier and is thought to have been 3-4 times wider than the modern Cascades (Priest, 1990). The Clarno Formation of central Oregon (Bestland, 1999), Siletz River, and Crescent Formations of Washington contain significant amounts of subaerial volcanic

rock that erupted as early as 51 Ma (Wells et al., 2014), suggesting some terrestrial settings existed by that time. The first plutons of the Cascade arc appeared at ~26 Ma (du Bray and John, 2011), with a significant volume of ignimbrites erupting from 39-18 Ma (Robinson et al., 1984) before volcanic activity slowed greatly between 17-10 Ma (Priest, 1990). In the mid-Miocene, the Columbia River Flood Basalt Group (CRBG) inundated much of Oregon and southern Washington (Sherrod and Smith, 2000; Beeson et al., 1989). The CRBG contains valley-filling basalt flows (Beeson et al., 1989) and thus reflects the topography at the time of deposition. CRBG thickness is heterogeneous, with a maximum thickness of 1.2km at Dog Mountain in southern Washington (Beeson et al., 1989). The CRBG are largely absent in the Cascades themselves, suggesting that the Cascades served as a topographic barrier at that time. It is also likely that CRBG has since been eroded and/or is buried beneath younger volcanic rocks. In the late Miocene, further volcanic activity is evidenced by ash deposition and volcaniclastics of the Deschutes Formation and widespread Rattlesnake Tuff (Smith et al., 1987; Streck and Grunder 1995).

2.3 Reconstructing Paleoenvironments using Stable Isotopes

Oxygen isotopes in paleosol carbonates ($\delta^{18}O$) reflect environmental soil water chemistry. As carbonates crystallize, they incorporate oxygen from soil water (Cerling and Quade, 1993). Carbonate cements and nodules form within thousands of years, so paleosol carbonates are thought to average environmental isotopes over this time (Garzione et al., 2000). Soil waters are typically dominated by meteoric water, so records of soil water are often used to infer ancient meteoric water (e.g. Quade et al., 2007;

Bershaw et al., 2012). In relatively arid, closed basin systems, evaporation can increase the $\delta^{18}O$ values of surface water (Gat and Airey, 2006). Therefore, many researchers focus on the lowest isotopic values from the rock record as a reflection of unevaporated precipitation (Mack et al., 2000). Alternatively, diagenetic alteration can result in anomalously negative isotopic values (Garzione et al., 2000). Therefore, it is important to identify primary, authigenic carbonates for paleoenvironmental interpretation.

Similarly, deuterium isotopes in volcanic glass (δD) have been shown to reflect environmental water of secondary hydration, which occurs on the scale of thousands of years post-deposition. (Ross and Smith, 1955; Friedman et al., 1993). Volcanic glass is thermodynamically unstable relative to mineral phases and thus prone to aqueous interactions such as hydration and alteration (Fisher and Schmincke, 1984). If the overall rock body which contains the glass is permeable enough for water interaction, water will diffuse into the glass structure (Friedman et al. 1993). As the water that interacts with newly deposited glass is most likely to be meteoric, hydrated volcanic glass has potential to preserve ancient meteoric water isotope signatures within the glass structure.

Deuterium excess (d-excess) is a second-order isotopic parameter that is a function of both $\delta^{18}O$ and δD, defined by the equation (Craig, 1961):

$$d\text{-}excess = \delta D - 8 * \delta^{18}O \quad [1]$$

It is sensitive to evaporation under relatively dry conditions (e.g. Gat and Carmi, 1970; Bershaw, 2018; Uemura et al., 2008). Humidity and d-excess are correlated in surface water, such that if d-excess decreases through time, it may be an indication of climate aridification (Rohrmann et al., 2016).

3.0 Methods

3.1 Sample Selection

I targeted paleosol carbonates ($\delta^{18}O$) and volcanic glass (δD) of Cenozoic age in central Oregon for paleoenvironmental analysis (Figure 1). This time period is the most represented in the geologic record, with the oldest paleosols and volcanic glass deposits being Eocene in age. More specifically, I focused on the early Miocene to Oligocene period because it is poorly represented in the published literature, particularly the Paleogene. Central Oregon was targeted due to its position in the lee of the modern Cascades, making it an optimal region to observe the development of a rain shadow due to topographic growth of the Oregon Cascades and Coast Range. Refer to Appendix B for detailed descriptions of outcrops and samples. Paleosol carbonates throughout the John Day Formation of known age (~30-16 Ma) were sampled based on locations described in Retallack et al. (1999) (red circles in Figure 1). Up to 100 grams of sample was collected after removing the upper 30 cm of outcrop to reduce the influence of modern water and evaporation. Bk horizons were targeted, as these are the horizons where carbonate concretions form readily. Care was taken to avoid diagenetically altered samples when possible, identified in the field by spar, calcite veins, and oxidation (e.g. Bershaw et al., 2012). Within a single outcrop, sampling was conducted at spacings of several meters true stratigraphic thickness.

Felsic volcanic ash samples were sampled with ages ranging from ~39-28 Ma, based on published radiometric ages (red squares in Figure 1, Appendix B). Samples were taken within a small area to minimize spatial variability within the Cascade rainshadow. When possible, bulk sample (>1 kg) was collected from 5-10 cm beneath

surface exposure. Sample number COS1903 was the only exception collected as float. It was likely derived from the underlying bedrock because it was on a narrow local topographic high. Outcrops were selected from sites previously described in the literature (Bestland et al., 2008; Retallack et al., 1999; McLoughry et al., 2009; Robinson et al., 1984) and were not pursued if they had not been described as “vitric”. Three samples collected by Carlson (2018) were analyzed for the first time and two of her samples were re-analyzed (Appendix B).

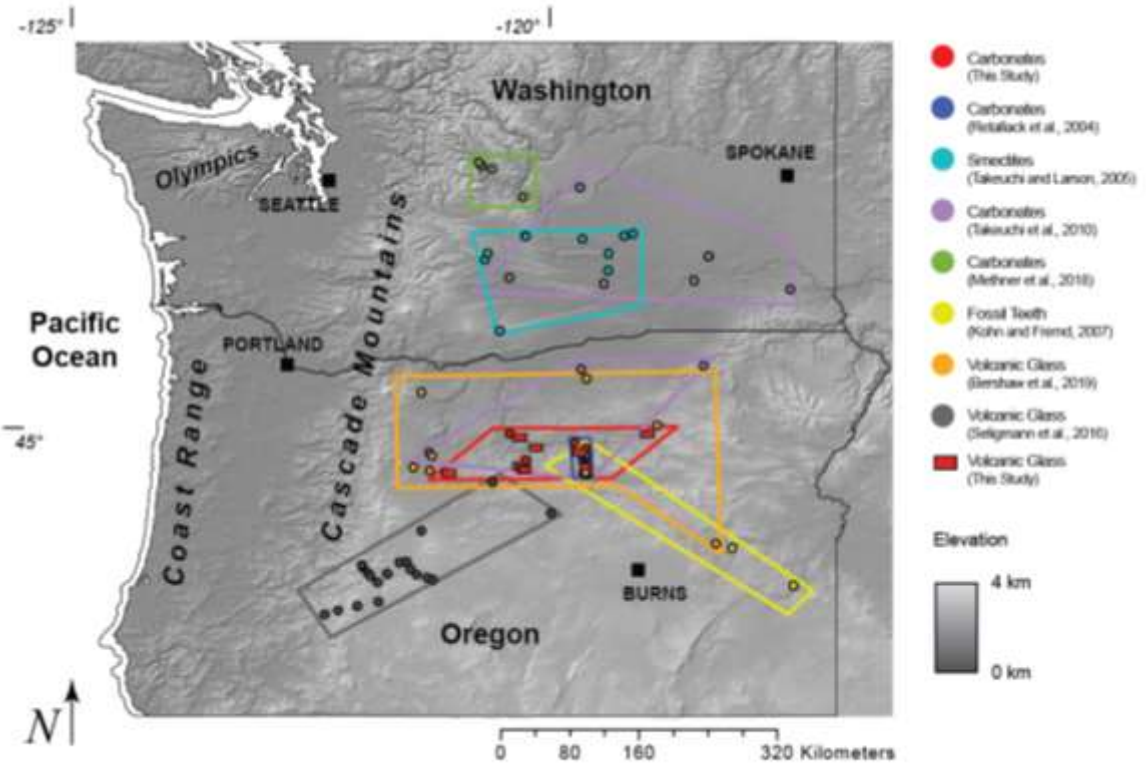

Figure 1. Location map showing the extent of new data (red) and published datasets throughout the Pacific Northwest. Elevation is shown as greyscale in km. Digital Elevation Model (DEM) is based on the U.S. Geological Survey Global 30 Arc-Second GTOPO30.

I combined my results with published data throughout the Pacific Northwest to more comprehensively characterize regional and temporal trends. This consists of the following $\delta^{18}O$ data: 172 paleosol carbonates from Washington and Oregon (Takeuchi et al., 2010), 367 paleosol carbonates from Oregon (Retallack, 2004), 22 smectites from Washington (Takeuchi and Larson, 2005), 243 fossil teeth from Oregon (Kohn and Fremd, 2007), 147 Palouse loess from Washington (Stevenson, 1997), 31 modern carbonates from Washington (Lechler et al., 2018), and 119 carbonate concretions from Washington (Methner et al., 2018) (Table S1). My synthesis also includes the following δD data: nine volcanic glass samples from central Oregon (Bershaw et al., 2019) and 25 Mazama ash samples (Seligmann et al., 2016) (Figure 1). Published modern stream water $\delta^{18}O$ values from Washington and Oregon are reported for comparison (Table S2).

3.2 Preparation and Analytics

3.2.1 Paleosol Carbonates

Samples were crushed to powder and reacted with 30% H_2O_2 to remove organics. Analyses were carried out at the Iowa State University Stable Isotope Lab (SIL) on a ThermoFinnigan Delta Plus XL mass spectrometer in continuous-flow mode via Thermo GasBench II with a CombiPal autosampler. The long-term precision of the mass spectrometer for $\delta^{18}O$ is 0.06‰. Isotopic results are reported in standard delta notation ($\delta^{18}O$) relative to Vienna Standard Mean Ocean Water (VSMOW) (Table S1).

3.2.2 Volcanic Glass

Volcanic glass sample preparation was designed to isolate δD values in volcanic glass shards found in ash samples (tuff) that reflect meteoric water within 10 ka of ash deposition. Protocol followed methods outlined in Bershaw et al. (2019) and Cassel and Breecker (2017). For each sample, ~500 grams were crushed with a ceramic mortar and pestle. Samples were then wet sieved to three size fractions (<70 um, 70-150 um, >150 um). Samples in the 70-150 um size fraction were given preference as larger grains (>150 um) have been shown to have an increased chance of magmatic hydrogen present (Seligman et al. 2016). To remove carbonates, samples were treated with 10% HCl and dried with a vacuum pump. Samples were then treated with 8% HF to remove surface precipitates and altered glass that is unlikely to reflect ancient meteoric water. Utilizing liquid lithium metatungstate (LMT), density gradients were created to separate minerals from glass. Specifically, separations were performed at 2.25 g/cm^3 (pumiceous glass from glass shards), and 2.56 g/cm^3 (glass shards from quartz and feldspar).

At each step, samples were checked for glass purity in oil immersion slides via petrographic microscope. Samples that were not yielding at least 99% purity were retreated with HF and/or LMT. Typically, impurity presented as either birefringence (suggesting the presence of minerals) in either normal or cross-polarized light, or by being extinct in normal light (indicating thorough alteration of the glass grain).

3.3 Estimating Paleo-water Isotopic Compositions and Deuterium Excess

In addition to new data, I synthesized stable isotope data from Washington and Oregon, including fossil teeth (Kohn and Fremd, 2007), paleosol carbonates (Takeuchi et

al., 2010; Retallack, 2004; Lechler et al., 2018), smectites (Takeuchi and Larson, 2005), and carbonate concretions (Methner et al., 2018) (Table S1).

To compare different proxy material, I converted stable isotope results to meteoric water using empirically derived fractionation factors (O'Neil et al., 1969; Yeh and Savin, 1977). These are a function of temperature, which I estimate from ancient flora (Wolfe, 1994). Carbonate concretions with Δ47 temperatures were used when available (Methner et al., 2018). Fossil tooth data was converted to water using an empirical relationship between environmental water and tooth chemistry (Kohn and Fremd, 2007).

Volcanic glass δD was converted to meteoric water using an empirical relationship described by Friedman et al. (1993). To estimate ancient d-excess (Eq. 1), I compare stable $\delta^{18}O$ values of meteoric water estimated from carbonates, smectites, and fossil teeth to δD values of contemporaneous water estimated from volcanic glass.

4.0 Results

4.1 New Carbonate Stable Isotope Data

I collected and analyzed 20 carbonate samples in central Oregon which I report here (Table 1, Figure 4). Sample ages were determined by comparing stratigraphic position with published ages based on radiometric dating of tuff beds (Retallack et al., 1999, Retallack, 2004). Exceptions are COS1907 and COS1907b, which are dated based on their position atop the Dayville Basalt (16.1 Ma) and below the Mascall Tuff Bed (15.2 Ma) (Bestland et al., 2008; Prothero et al., 2006; Drewicz and Kohn, 2018). There is a weak positive correlation between $\delta^{18}O$ and latitude (R^2 of 0.32) and no significant relationship between $\delta^{18}O$ and longitude, elevation, or sample age (R^2 of 0.01, 0.19, 0.00, respectively). The average $\delta^{18}O$ value of my carbonate samples, which are between 32.7-15.6 Ma in age, is -11.2‰ with a range from -14.6‰ to -7.0‰. This average is 1.6‰ more positive than the average of modern meteoric water in the lee (east) of the Oregon Cascade Mountains (-12.8‰), but within the range (-16.2‰ to -8.8‰) (Table S2).

4.2 New Volcanic Glass Stable Isotope Data

I collected and analyzed seven new volcanic glass samples and analyzed five samples by Carlson (2018), 3 of which (CVG033, CVG034, and CVG037) were not previously analyzed and two which were reruns (CVG013, CVG036) (Table 1). The average δD for all samples is -80.2‰ with a range of -136.6‰ to -51.0‰. There is no apparent correlation between δD and latitude or δD and age (R2 of 0.00 and 0.14, respectively) (Appendix C). δD is ~50‰ higher in Paleogene (average = -72.1‰)

samples than Neogene (average = -121.1‰), with the exception of the 32.7 Ma Tuff of Dale sample (-118.9‰). There is a weak, negative correlation between δD and longitude (R2=0.21) and between δD and modern elevation (R2=0.34) (Appendix C).

Table 1. Compilation of samples tested for this study

Name/Formation	Sample ID	Type	Age (Ma)	Latitude	Longitude	δ180 (Rock) (‰)	δ180 (Water) (‰)	δD (Rock) (‰)	δD (Water) (‰)	Elevation (m)
Mascall	CVG033	Glass	15.2	44.50	-119.61			-165.1	-136.6	690
Mascall	CVGO34	Glass	15.2	44.50	-119.63			-135.2	-105.7	690
Sanidine Tuff	CO51905	Glass	28.5	44.66	-120.27			.88	-56.9	603
John Day Fm. Member A	CO51918	Glass	39.8	44.93	-120.43			-92.5	-61.5	635
John Day Fm. Member A	CVG037	Glass	39.8	44.80	-120.17			-112.9	-82.6	696
Tuff of Smith Rock	COS1902	Glass	29.5	44.50	-121.16			-107	-76.5	863
Picture Gorge Ignimbrite	COS1903	Glass	26.94	44.66	-120.27			-96.3	-65.5	727
Picture Gorge Ignimbrite	COS1910	Glass	26.94	44.66	-119.64			-86.7	-55.5	642
Picture Gorge Ignimbrite	COS1910	Glass	26.94	44.66	-119.64			-82.3	-51.0	642
Picture Gorge Ignimbrite	COS1910	Glass	26.94	44.66	-119.64			-92.8	-61.8	642
Picture Gorge Ignimbrite	CVG036	Glass	26.94	44.66	-120.26			-108.4	-78.0	641
Tuff of Dale	CVG013	Paleosol Car	32.66	45.01	-118.89			-159.9	-131.2	1924
Turtle Cove	COS1904	Paleosol Car	28.65	44.66	120.25	21.2	-9.7			610
Turtle Cove	COS1905	Paleosol Car	29	44.66	120.27	19.4	-11.5			603
Turtle Cove	COS19011	Paleosol Car	30	44.6	119.64	16.1	-14.6			693
Turtle Cove	COS1912	Paleosol Car	30	44.66	119.64	19.7	-11.2			693

Table 1 continues on next page

Table 1 Continued

Name/Formation	Sample ID	Type	Age (Ma)	Latitude	Longitude	δ180 (Rock) (‰)	δ180 (Water) (‰)	δD (Rock) (‰)	δD (Water) (‰)	Elevation (m)
Kimberly	COS1913	Paleosol Car	23.35	44.77	119.63	19.4	-11.4			609
Kimberly	COS1914	Paleosol Car	23.05	44.77	119.63	17.6	-13.2			609
Kimberly	COS1915	Paleosol Car	22.64	44.77	119.63	19.9	-11.0			609
	COS1907	Paleosol Car	15.6	44.51	-119.66	17.7	-13.5			782
	COS1907b	Paleosol Car	15.6	44.51	-119.66	18.4	-12.7			782
Haystack Valley	JDRL08	Paleosol Car	20.4	44.84	119.75	24.0	-7.0			559
Haystack Valley	JDRL05	Paleosol Car	20.9	44.84	119.74	19.1	-11.8			559
Turtle Cove	JDRL04	Paleosol Car	28.7	44.55	119.64	20.5	-10.4			725
Haystack Valley	JDRL06	Paleosol Car	20.77	44.84	119.74	17.8	-13.0			559
Big Basin	JDRL02	Paleosol Car	32.7	44.56	119.64	11.8	-17.9			561
Big Basin	JDRL02	Paleosol Car	32.7	44.56	119.64	11.2	-18.5			561

The average wt.% H_2O is 2.72% with an overall range from 0.57% to 7.54% (Figure 2). There is no apparent relationship between water content and latitude, longitude, age, or modern elevation (R^2 of 0.00, 0.04, 0.00, and 0.00, respectively) (Appendix C). The relationship between water content and δD correlates weakly (R^2=0.27), and becomes stronger with the removal of a single outlier (Sample CVG037) (R^2=0.50) (Figure 2). Similarly, the relationship between water content and age does not correlate (R^2=0.00), but does with the removal of CVG037 (R^2=0.42) (Appendix C).

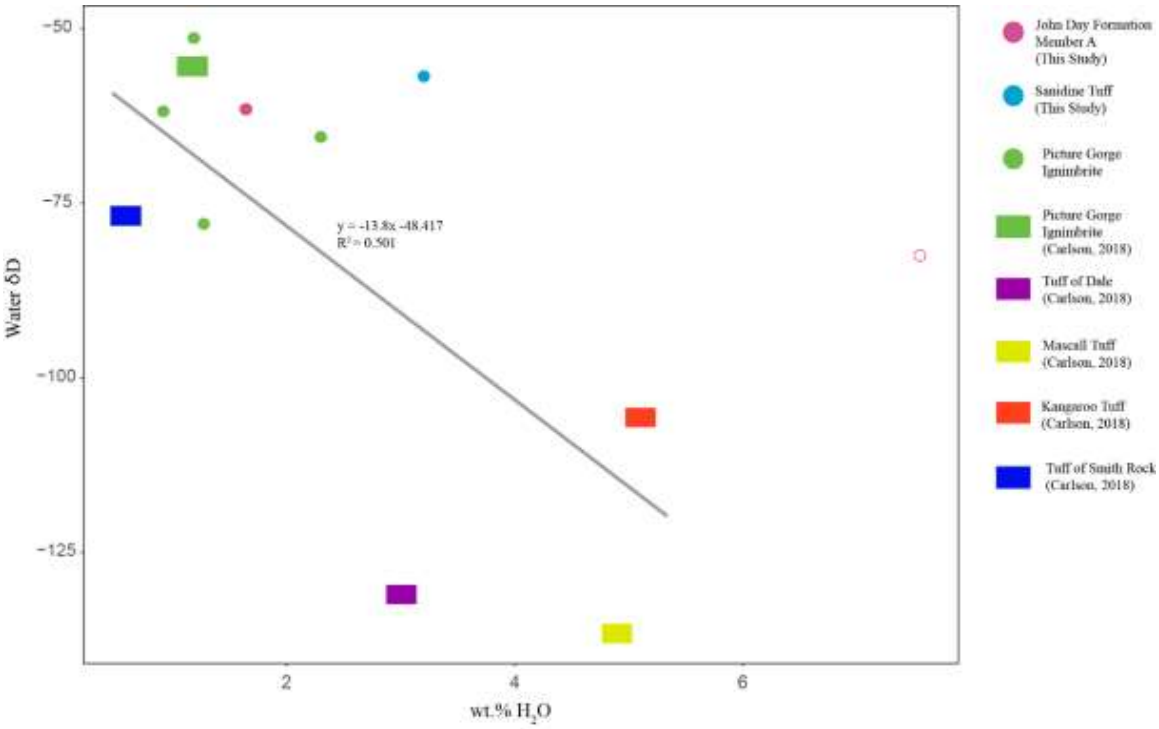

Figure 2. Plot showing relationship between wt.% H_2O and water δD in volcanic glass samples from central Oregon. Open circle represents an outlier which is not considered in the linear regression. Squares indicate samples collected by Carlson (2018) which I analyzed in this study.

4.3 Synthesis of Published Data

Taken as a whole, my paleosol carbonates $\delta^{18}O$ data combined with published datasets do not show significant relationships with latitude, longitude, elevation, or age (R^2 of 0.15, 0.00, 0.22, and 0.13, respectively) (Appendix C). This is also the case with volcanic glass, which similarly does not show significant correlation between δD and latitude, longitude, elevation or age (R^2 of 0.00, 0.00, 0.13, 0.00, respectively) (Fig 3, Appendix C).

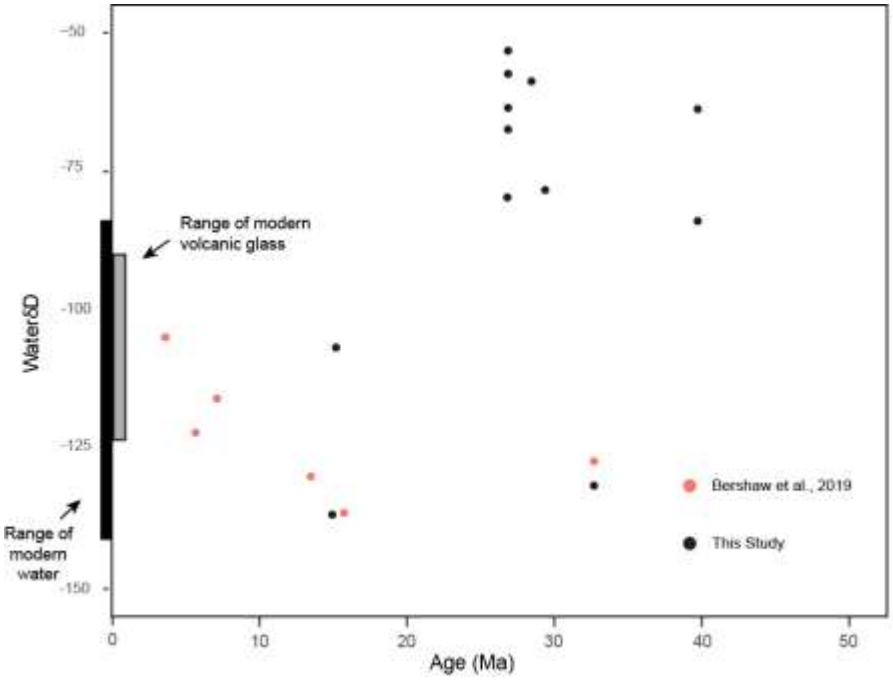

Figure 3. Plot showing temporal variations in water δD of volcanic glass in Central Oregon. Modern volcanic glass (gray bar) is from Seligmann et al. (2016). See Figure 1 for dataset locations and Table S2 for modern water dataset.

I separate datasets by state, as this provides a convenient latitudinal break between the northern Cascades of Washington and central Cascades of Oregon. In Washington, the average $\delta^{18}O$ for all samples is -14.3‰ ± 2.8‰ (1σ SD) and range from -18.0‰ to -6.8‰. There is a weak, negative correlation between age and $\delta^{18}O$ in samples

from Washington, with an R^2 of 0.40. The average $\delta^{18}O$ in Oregon is -11.9‰ ± 2.1‰ (1σ SD), ~2.4‰ more positive than Washington, with a range of -15.8‰ to -8.4‰. Oregon carbonates demonstrate negligible correlation between age and $\delta^{18}O$ (R^2 of 0.03). Sample $\delta^{18}O$ values from individual studies are averaged within 2.5 million-year bins to emphasize trends in climate and topography across geologic time (Figure 4).

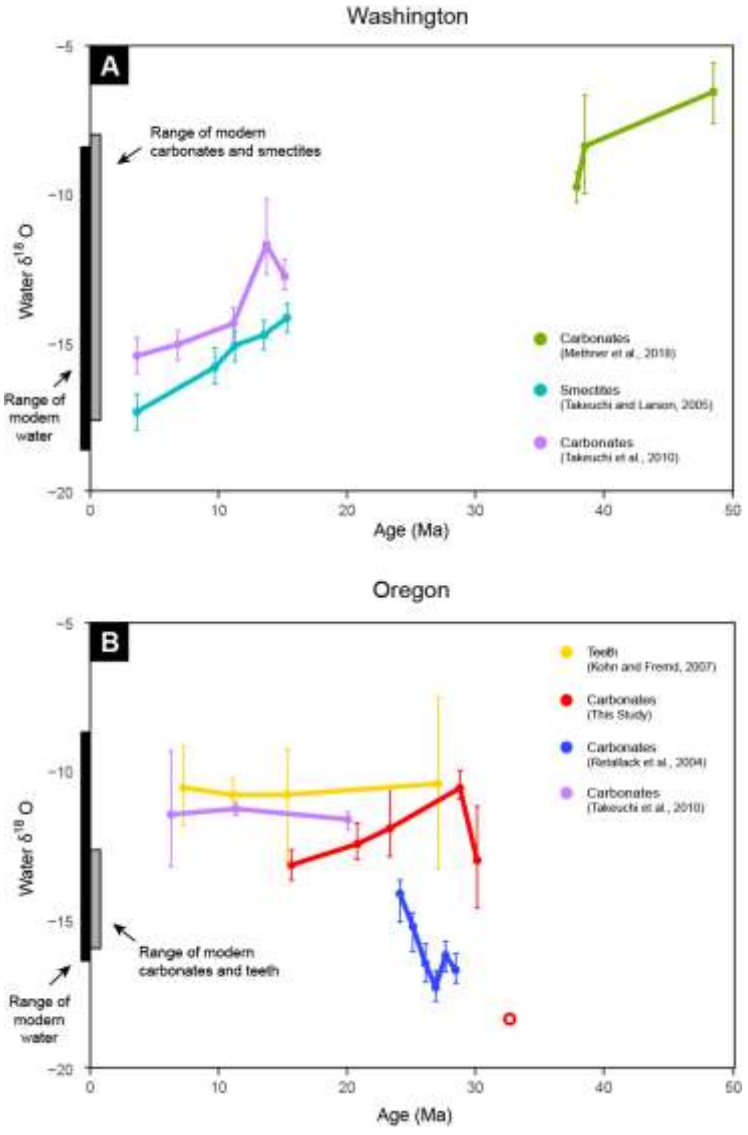

Figure 4. Plots showing temporal variations in meteoric water based on $\delta^{18}O$ values of carbonates, smectites, and fossil teeth for central Washington at ~47° latitude (A) and central Oregon at ~45° latitude (B), both in the lee (east side) of the Cascade Mountains. Modern water data provided in Table S2.

5.0 Discussion

5.1 Carbonates as a Proxy for Ancient Meteoric Water

Before interpreting geologic and climatic trends, I assess whether proxies from the rock record accurately reflect meteoric water at the time of deposition. Several paleosol carbonate samples from central Oregon likely experienced some form of alteration which would shift $\delta^{18}O$ from their original meteoric water derived values. One Oligocene sample from my dataset (JDRL02) has an anomalously low $\delta^{18}O$ value (-18.2‰) (open red circle in Figure 4B) This sample is purple in hue and only weakly calcareous, so it is likely that it underwent oxidation that obfuscates the isotopic signal. In addition, pedogenic carbonate $\delta^{18}O$ values from Retallack (2004) across the late Oligocene (blue curve in Figure 4B) plot more negative (~5‰) than roughly contemporaneous fossil teeth and paleosols. If the mineralizing fluids consisted of meteoric water, but the temperature of carbonate formation was significantly higher (e.g. Methner et al., 2018), fractionation would result in relatively negative carbonate $\delta^{18}O$ values. The Turtle Cove Member, which makes up samples 24 Ma and older (Retallack, 2004), contains significant amounts of celadonite, which is an alteration product that forms between 27°C and 100°C at depth (Lander and Hay, 1993; Weaver, 1989). Alteration may have affected the paleosol carbonate, rendering a different stable isotope signature. While Hay (1963) provides a narrower range of water temperatures for this interaction (27-55°C) and an age estimate of when this occurred (24±2 Ma), this temperature range may produce up to 5‰ variability in carbonate $\delta^{18}O$.

5.2 Volcanic Glass as a Proxy for Ancient Meteoric Water

None of the volcanic glass samples newly analyzed for this study appear to reflect ancient meteoric water. Samples with < 2 wt. % H_2O are interpreted to be influenced by magmatic water. Magmatic water is typically between -90‰ to -30‰ (Friedman et al., 1993; Seligman et al., 2016). This is enriched relative to typical surface waters in the region, which range from -138‰ to -67‰ (Table S2). Volcanic glass comprises ~0.2-0.6 wt. % H_2O following degassing (Friedman, et al., 1993), so samples containing < 2 wt. % H_2O can be >30% magmatic. The average paleowater δD of my volcanic glass samples with wt. % H_2O < 2 is -64.4‰, which is significantly higher than is expected of modern water (average= -109‰) and more in line with magmatic, so it is unlikely these samples are accurately recording paleowater. This trend is further demonstrated by a correlation between δD and wt. % H_2O (R^2 = 0.50), when outlier CVG037 is excluded (Figure 2). This suggests that the less water in the sample, the larger the magmatic influence.

The outlier (CVG037) shows a significantly higher wt. % H_2O (7.54%) and δD value (-82.6‰). It may represent lacustrine waters which could allow for thorough hydration of the rock, and impart δD values that are relatively enriched compared to meteoric water (Cassel et al., 2014; Dansgaard, 1964). Similarly, though sample COS1903 is 2.3% H_2O by weight, the δD (-65‰) value is still much higher than is typical for modern meteoric water in the region, suggesting it may also have been hydrated by relatively enriched surface water, and/or influenced by magmatic water. Other samples of the same formation all reported wt. % H_2O values < 1.2 and δD values that are relatively high (average = -58‰).

Lastly, the 28.5 Ma Sanidine Tuff (COS1905) has a wt. % H_2O of 3.2 and a water δD of -56.9‰, which is also significantly higher than modern precipitation. It is likely high due to alteration of the glass surface, as it was not possible to reach >99% glass purity in this case. Surface precipitates typically reflect relatively modern meteoric water values, as the precipitates would gain and lose water to the surrounding meteoric water (Gin et al., 2015). Since the actual composition of surface precipitate and amount of surface precipitate on the glass itself is variable, so is the impact it has on stable isotope data. Experimental data suggest that surface precipitates can push stable isotope data from +12‰ to -34‰ (Dettinger and Quade, 2015) with same age samples from the same location having variations in δD of up to 37‰ (Seligman et al., 2016). For these reasons, I interpret the reported δD as reflective of the surface precipitate, not glass δD.

5.3 Interpretation of New Carbonate Data

My carbonate data (red curve in Figure 4B) are within the wide range of modern meteoric water (dark vertical bar in Figure 4B) in the Oregon Cascade rainshadow, suggesting that some topography, possibly similar to modern, existed by the late Oligocene. I observe a depletion in carbonate $\delta^{18}O$ of ~2.5‰ in my data (red curve) from ~29 Ma to ~16 Ma. This could be due to modest topographic uplift of the Oregon Cascades at this time, culminating in the eruption of CRBG in the mid-Miocene (Beeson et al., 1989; Barry et al., 2013; Reidel et al., 2013). My interpretation of relatively high topography in the Oregon Cascades by Oligocene time is consistent with evidence of significant volcanism (Verplanck and Duncan, 1987; Priest, 1990; Taylor, 1990; Conrey et al., 1997) and volcanic glass δD data across the range (Bershaw et al., 2019). A

decrease in global oceanic $\delta^{18}O$ of ~1‰ from the late Oligocene to the mid-Miocene climatic optimum (Zachos et al., 2001) could account for some of my observed decrease in carbonate $\delta^{18}O$. However, warmer temperatures would largely offset this effect.

5.4 Regional Synthesis: Oregon

In my regional synthesis, I do not consider carbonates from Retallack et al. (2004) (blue curve in Figure 4B), or my sample JDRL_02 (open red circle in Figure 4B), as there is evidence that they are diagenetic (Refer to Section 5.1 for details), though Retallack (2004) interprets them as accurately reflecting Milankovitch-scale changes in global climate. My time-averaged carbonate data is within ~2.4‰ of other water proxy data in Oregon. This isotopic variability in paleowater proxy material is similar to that observed in modern soils and teeth (gray vertical bar in Figure 4B), and smaller than the variability observed in modern meteoric water nearby (black vertical bar in Figure 4B). Ancient, non-diagenetic carbonate $\delta^{18}O$ values (average -12.1‰) are significantly more negative than modern coastal meteoric water in Oregon, which is about -6.8‰ (Bershaw et al., 2020). This suggests there has been some topography associated with the Oregon Cascade Mountains, possibly similar to modern, since at least late Oligocene time. Though my data show a modest decrease in $\delta^{18}O$ during the early Miocene, when considered with other proxy data, it seems likely that regional climate and topography was relatively stable during this time. Spatial variability among sample locations within the study area (Figure 1) is likely causing modest discordance among proxy data, similar to observations of modern meteoric water across the same spatial extent (Table S2 and Bershaw et al., 2020).

Fossil tooth (Kohn and Fremd, 2007) and paleosol carbonate (Takeuchi et al., 2010) $\delta^{18}O$ values from the late Miocene and Pliocene are 2-3‰ more positive than modern carbonates and teeth (Figure 4B) in central Oregon. This is likely not caused by global cooling at this time, as northern hemisphere ice sheet expansion resulted in a ~1.5‰ increase in oceanic $\delta^{18}O$, largely offsetting any cooling effect (Zachos et al., 2001). Instead, this negative shift in isotopic composition since the late Miocene may reflect the westward migration of the Oregon coast, driven by the Neogene emergence of a subaerial Oregon Coast Range (Figure 5). A drop in $\delta^{18}O$ values would be expected as the distance to the Pacific Ocean increased and a subaerial Coast Range created a modest moisture barrier, further depleting ^{18}O in vapor. Emergence of the Coast Range at this time is independently constrained by basin analysis of the Portland Basin, which shows a significant decrease in accommodation space sometime after the eruption of the CRBG in the mid-Miocene and coeval migration of basin depocenters eastward (Scanlon, 2019). Additionally, submarine, tholeiitic basalts have been mapped in the Coast Range as young as <16 Ma (Snavely et al., 1973), further supporting coast line migration from the late-Miocene to now. Modern coastal meteoric water $\delta^{18}O$ values are ~2.4‰ higher than those in the western foothills of the Cascade Mountains (Bershaw et al., 2020), where the coastline was prior to Coast Range uplift. This suggests that uplift of the Coast Range could account for the discrepancy between late Miocene and modern water proxy data.

5.5 Regional Synthesis: Washington

Estimated meteoric water $\delta^{18}O$ values from Eocene carbonates in Washington (Methner et al., 2018) are relatively positive (average -8.8‰) compared to both modern

water (average -14.6‰) and modern carbonates and smectites nearby (average -14.0‰) (Figure 4A and Table S1). Instead, they are similar to the isotopic composition of modern stream water at low elevations on the west side of the Olympics (-7.1‰) and Cascades in Washington (-9.1‰) (Bershaw et al., 2020), suggesting the northern Cascades Mountains were not a significant topographic barrier to westerly-derived moisture at that time. Eocene paleowater $\delta^{18}O$ values are also significantly more positive than Miocene and Pliocene smectite and paleosols (Figure 4A), showing a progressive trend towards more negative $\delta^{18}O$ values across the Cenozoic. This trend is not likely the result of global cooling, as temperature change is moderated by an increase in oceanic $\delta^{18}O$ of ~1.8‰ from the late Eocene to Miocene (Zachos, 2001). I hypothesize that the northern Cascades in Washington have undergone steady topographic uplift since the middle Eocene, causing a progressive decrease in $\delta^{18}O$ values during that time. This interpretation is consistent with independent evidence that the northern Cascades were an active volcanic arc in the Paleogene (Tabor et al., 1984) and thermochronology that shows slow uplift of the Washington Cascades (<0.25 km/m.y.) from the Eocene to the late Miocene (Reiners et al., 2002; Pesek et al., 2020), with ongoing uplift today at a quicker rate (0.5-1 km/m.y.) (Wells and McCaffrey, 2013; Reiners et al., 2002).

5.6 Polygenetic History of Topography across the Pacific Northwest

My synthesis of water proxy datasets suggests a polygenetic uplift history for the Cascade Mountains along strike (Figure 5). Oregon and Washington carbonates generally show distinct temporal trends, with differences as large as ~5‰ across the late Miocene, where Oregon paleowaters are more enriched than contemporaneous water in

Washington (Figure 4). These spatial discrepancies support my assertion that global climate change is not the primary forcing mechanism behind isotopic change in the Pacific Northwest. Instead, isotopic proxy records suggest that the Northern Cascades in Washington have been experiencing progressive topographic uplift from the middle Eocene to today, while the Cascades in Oregon formed a topographic barrier by the late Oligocene, but remained relatively unchanged into the Neogene. This is consistent with the tectonic framework of the region since mid-Miocene time, where rigid block rotation has resulted in north-south shortening (uplift) of the northern Cascades against a relatively stable Canadian buttress (Wells et al., 1998; McCaffrey et al., 2013), while east-west extension (subsidence) has developed in the Oregon Cascades (Guffanti and Weaver, 1988; Conrey et al., 1997). A polygenetic uplift history of the Oregon and Washington Cascades has also been proposed by Bershaw et al. (2019) based on volcanic glass δD values and Pesek et al. (2020) based on thermochronometry, which shows significant geographic variation in exhumation timing, as opposed to contemporaneous, wholesale uplift of the entire Cascade Mountain chain.

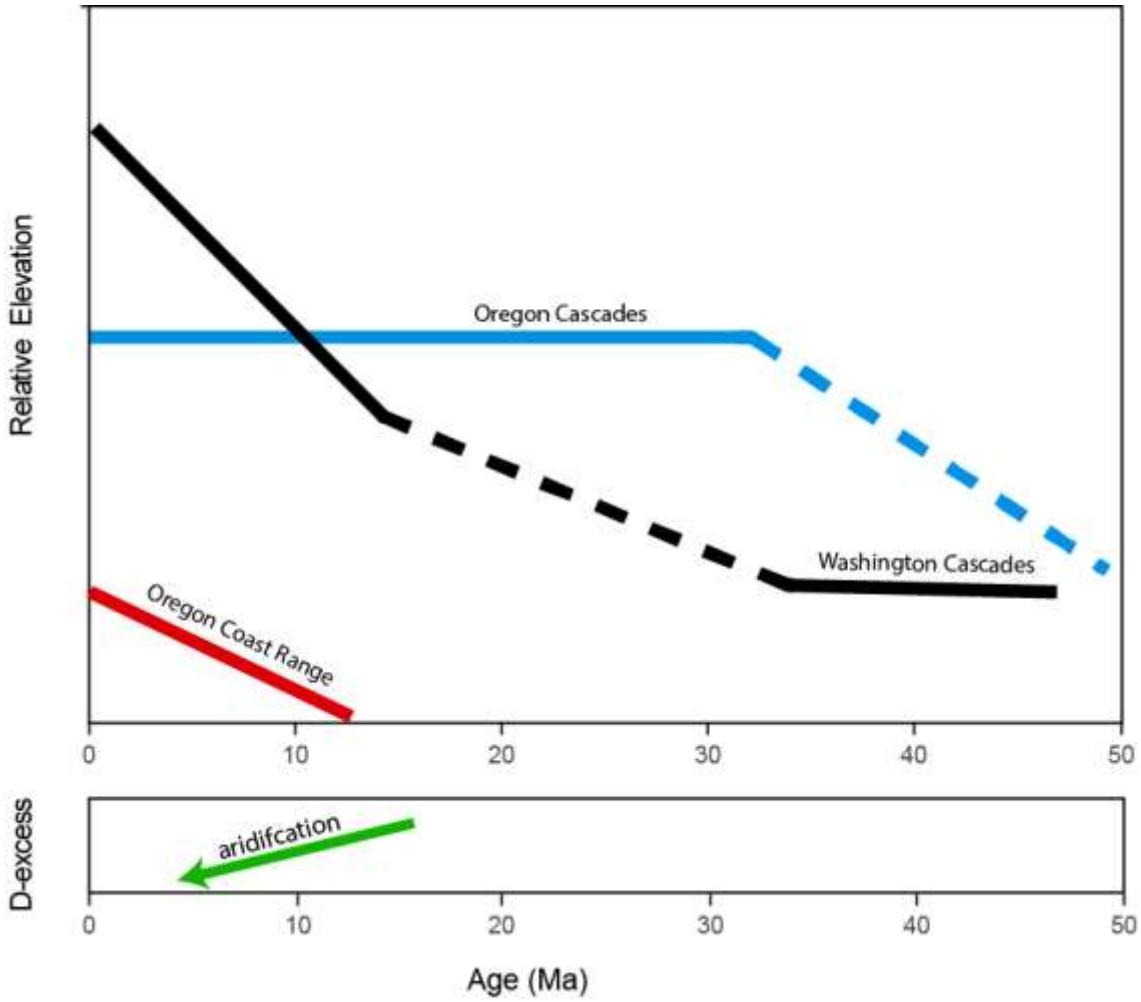

Figure 5 Plots showing change in relative elevation above sea level (upper) over time and relative change in d-excess (lower) for central Oregon over time. D-excess is a proxy for aridity, with lower values associated with more arid conditions, suggesting that central Oregon became more arid as the Oregon Coast Range emerged and coastline migrated westward. Dashed lines indicate periods where no stable isotope proxy data exists and solid lines indicate time periods with stable isotope proxy data included in this study.

Additionally, I hypothesize that the subaerial emergence of the Coast Range in Oregon and westward migration of the coastline (Scanlon, 2019) caused a modest depletion in proxy material $\delta^{18}O$ values that is not apparent in Washington proxy data, where the coastline (Puget Sound) remains at the base of the northern Cascades today.

5.7 Ancient D-Excess and Paleo-aridity

I compare Oregon carbonate $\delta^{18}O$ data to contemporaneous Oregon volcanic glass δD data (Bershaw et al., 2019) to constrain ancient d-excess in central Oregon across the Miocene. Generally, volcanic glass δD becomes more positive from the mid-Miocene to modern, while $\delta^{18}O$ becomes more negative from the late Miocene to modern (Figures 3 & 4). Assuming that these samples reflect contemporaneous meteoric water, this would suggest that ancient d-excess decreases over that time, which I interpret as aridification from a more humid environment during the Miocene (Figure 5). This agrees with paleontological and pedological observations that suggest relative humidity may have been 10% higher at 15-16 Ma relative to today (Retallack, 2004; Bestland et al., 2001). Based on modeling of the relationship between d-excess and relative humidity, a 10% change in relative humidity at the moisture source would result in a 6‰ increase in d-excess for evaporated vapor (Merlivat and Jouzel, 1979). This is similar to the difference in d-excess from ~15.5 Ma to ~7 Ma, which is ~8‰ in these samples.

However, calculated d-excess values are between 40‰ and 32‰, much higher than modern waters. This discrepancy may be due to uncertainty in the fractionation equation for volcanic glass (e.g. Friedman et al., 1993) as multiple independent $\delta^{18}O$ proxies are consistent with each other (Figure 4) and are calculated as a function of temperature, whereas the fractionation equation for volcanic glass (δD) does not incorporate temperature. Regardless, any errors in the fractionation equation for volcanic glass would affect all samples similarly. This means that even if d-excess values themselves are inaccurate, reconstructed d-excess trends are likely more reliable.

5.8 Opportunities for Future Research

Influence of Temperature on Volcanic Glass Fractionation

The fractionation equation of Friedman et al. (1993) is not a function of temperature. Ash temperature is highly variable throughout the hydration process and is related to initial deposition temperature and timing, unit thickness, and degree of burial (Fisher and Schmincke, 1984). As fractionation is a function of bond-strength, itself a representation of energy input requirements to break and reform atomic bonds, it is reasonable to expect that temperature should be considered in hydrogen isotope fractionation within volcanic glass. Martin et al. (2017) suggest that ash deposits remain at high temperatures for hundreds of years which can significantly accelerate the hydration process with meteoric water, increasing the potential for Milankovitch-scale influence on the isotopic signal. Gaining a better understanding of volcanic glass fractionation will make comparing volcanic glass to other paleoclimate proxies more effective, increasing the utility of ancient deuterium excess as a paleoclimate tool.

Understanding the Influence of Magmatic Water

Volcanic glass samples which were exceptionally enriched and low in wt. % H_2O were deemed too influenced by magmatic water to provide a reliable meteoric signal. Seligmann et al., (2016) created a model on the basis of mass balance relations to estimate meteoric water δD in low wt. % H_2O tephra. This requires knowledge of the volcano that erupted the ash and multiple sequences of eruptions from the same geologic section. A better understanding of the magmatic contribution to volcanic glass with low wt. % H_2O will clarify paleoenvironmental interpretations in this region.

Different Types of Hydrating H_2O

In the Cascades lee side and the Pacific Northwest as a whole, much of the year's precipitation comes in the winter. This quite often is snow, which fractionates differently than rainwater (Friedman et al., 1964). This is likely more significant in the Neogene than Paleogene, as humidity and temperature have been decreasing since the Oligocene (Retallack et al., 1999). Reassessing samples with snow as the source of meteoric waters in younger samples may affect paleoenvironmental interpretations.

Modeling Non-Perpendicular Airflow

The southwesterly Pineapple Express provides significant moisture in the Pacific Northwest during winter months (Dettinger, 2004). Therefore, there is a north-south component to moisture transport which means topography to the south of the study area may have a significant influence on stable isotopes of meteoric water. Adjusting airflow models accordingly may more faithfully recreate paleoenvironmental records of the region.

Different Pacific Northwest Topography

The Klamath Mountains and Blue Mountains of Oregon both have their own rainshadows which developed over geologic time. In fact, the Blue Mountains strike perpendicular to the direction of pineapple express moisture transport (Robinson et al., 1984). Performing stable isotope reconstructions of topography (paleoaltimetry) targeting these particular mountain ranges may lead to a better understanding their respective uplift

histories as well as clarifying the Cascades uplift history.

Deuterium From Single Units

The isotopic composition of volcanic glass is sensitive to several different factors besides topography and climate. Sampling contemporaneous units that are spatially variable may lead to a better understanding of competing depositional factors that may influence the isotopic composition of volcanic glass. Geochemical composition, texture, and degree of welding all have been shown to influence volcanic glass isotopes (Cassel and Breecker, 2017; Nolan and Bindemann, 2013). Analyzing and modeling the role of these factors in a single ash unit that is geographically widespread and texturally diverse may further elucidate ancient climate and topography.

6.0 Conclusions

I present new pedogenic carbonate $\delta^{18}O$ and volcanic glass δD data from central Oregon and synthesize this with published water proxy data from across the Pacific Northwest. I interpret a polygenetic history of Cascade Mountain topographic uplift along-strike, characterized by: 1) steady uplift of the Washington Cascades through the Cenozoic due long-term arc rotation and shortening against a Canadian buttress, and 2) uplift of the Oregon Cascades to similar-to-modern elevations by the late Oligocene, followed by topographic stagnation as extension developed into Neogene time. Since the Miocene, meteoric water $\delta^{18}O$ values have decreased in Oregon, possibly due to emergence of the Coast Range and westward migration of the coastline. Multi-proxy estimates of ancient d-excess are consistent with aridification in central Oregon during this time. This late isotopic shift is not seen in Washington as the Puget Lowland (Seattle) is still connected to the ocean, unlike the Willamette Valley in Oregon (Portland). Lastly, variability in $\delta^{18}O$ values of proxy material at any given time is likely related to variability inherent in arid environments (rainshadow) and/or the influence of Milankovitch-scale climate change.

References

Barry, T. L., Kelley, S. P., Reidel, S. P., Camp, V. E., Self, S., Jarboe, N. A., & Wolff, J. A. (2013). Eruption chronology of the Columbia River Basalt Group. The Columbia River Flood Basalt Province. Geological Society of America Special Paper, 497, 45-66.

Beeson, M. H., Tolan, T. L., & Anderson, J. L. (1989). The Columbia River Basalt Group in western Oregon; geologic structures and other factors that controlled flow emplacement patterns. Reidel, SP and Hooper, PR, Volancism and Tectonism in the Columbia River Flood-Basalt Province: Geological Society of America Special Paper, 239, 223-246.

Bestland, E. A., Forbes, M. S., Krull, E. S., Retallack, G. J., & Fremd, T. (2008). Stratigraphy, paleopedology, and geochemistry of the middle Miocene Mascall Formation (type area, central Oregon, USA). PaleoBios, 28(2), 41-61.

Bestland, E. A., Hammond, P. E., Blackwell, D. L. S., Kays, M. A., Retallack, G. J., & Stimac, J. (1999). Geologic framework of the Clarno Unit, John Day Fossil Beds National Monument, central Oregon. Oregon Geology, 61(1), 3-19.

Bershaw, J., Cassel, E. J., Carlson, T. B., Streig, A. R., & Streck, M. J. (2019). Volcanic glass as a proxy for Cenozoic elevation and climate in the Cascade Mountains, Oregon, USA. Journal of Volcanology and Geothermal Research, 381, 157-167.

Bershaw, J., Garzione, C.N., Schoenbohm, L., Gehrels, G., and Tao, L. (2012). Cenozoic evolution of the Pamir plateau based on stratigraphy, zircon provenance, and stable isotopes of foreland basin sediments at Oytag (Wuyitake) in the Tarim Basin (west China). Journal of Asian Earth Sciences, v. 44, p. 136–148, doi: 10.1016/j.jseaes.2011.04.020

Bershaw, J., Hansen, D. D., & Schauer, A. J. (2020). Deuterium excess and ^{17}O-excess variability in meteoric water across the Pacific Northwest, USA. Tellus B: Chemical and Physical Meteorology, 72(1), 1-17.

Bershaw, J., Penny, S. M., & Garzione, C. N. (2012). Stable isotopes of modern water across the Himalaya and eastern Tibetan Plateau: Implications for estimates of paleoelevation and paleoclimate. Journal of Geophysical Research: Atmospheres, 117(D2).

Bershaw, J. (2018). Controls on deuterium excess across Asia. Geosciences, 8(7), 257.

Carlson, T. B. (2018). Volcanic Glass as a Paleoenvironmental Proxy: Comparing Preparation Methods on Ashes from the Lee of the Cascade Range in Oregon, USA. [Master's Thesis]. [Portland, Oregon]: Portland State University

Cassel, E.J., and Breecker, D.O. (2017) Long-term stability of hydrogen isotope ratios in hydrated volcanic glass: Geochimica et Cosmochimica Acta, v. 200, p. 67–86, doi: 10.1016/j.gca.2016.12.001

Cassel, E. J., Breecker, D. O., Henry, C. D., Larson, T. E., & Stockli, D. F. (2014). Profile of a paleo-orogen: High topography across the present-day Basin and Range from 40 to 23 Ma. Geology, 42(11), 1007-1010.

Cerling, T. E., & Quade, J. (1993). Climate change in continental isotopic records. Geophysical Monograph, 78, 217-231.

Conrey, R. M., Sherrod, D. R., Hooper, P. R., & Swanson, D. A. (1997). Diverse primitive magmas in the Cascade arc, northern Oregon and southern Washington. The Canadian Mineralogist, 35(2), 367-396.

Craig, H. (1961). Isotopic variations in meteoric waters. Science, 133(3465), 1702-1703.

Currie, B. S., Polissar, P. J., Rowley, D. B., Ingalls, M., Li, S., Olack, G., & Freeman, K. H. (2016). Multiproxy paleoaltimetry of the late Oligocene-Pliocene Oiyug basin, southern Tibet. American Journal of Science, 316(5), 401-436.

Dansgaard, W. (1964). Stable isotopes in precipitation. Tellus, 16(4), 436-468.

Dettinger, M. D. (2004). Fifty-two years of “pineapple-express” storms across the West Coast of North America. US Geological Survey, Scripps Institution of Oceanography for the California Energy Commission, PIER Project Rep. CEC-500-2005-004, 20.

Dettinger, M. P., & Quade, J. (2015). Testing the analytical protocols and calibration of volcanic glass for the reconstruction of hydrogen isotopes in paleoprecipitation. Geological Society of America Memoirs, 212, 261-276.

Drewicz, A. E., & Kohn, M. J. (2018). Stable isotopes in large herbivore tooth enamel capture a mid-Miocene precipitation spike in the interior Pacific Northwest. Palaeogeography, Palaeoclimatology, Palaeoecology, 495, 1-12.

du Bray, E. A., & John, D. A. (2011). Petrologic, tectonic, and metallogenic evolution of the Ancestral Cascades magmatic arc, Washington, Oregon, and northern California. Geosphere, 7(5), 1102-1133.

Fisher, R. V, and Schmincke, H.U. (1984) Pyroclastic Rocks. Springer Science and Business Media.

Friedman, I., Gleason, J., Sheppard, R., and Gude, A. (1993). Deuterium Fractionation as Water Diffuses into Silicic Volcanic Ash: Climate Change in Continental Isotopic Records, p. 321–323.

Friedman, I., Sigurgeirsson, T., & Gardarsson, Ö. (1963). Deuterium in Iceland waters. Geochimica et Cosmochimica Acta, 27(6), 553-561.

Garzione, C. N., Quade, J., DeCelles, P. G., & English, N. B. (2000). Predicting paleoelevation of Tibet and the Himalaya from δ18O vs. altitude gradients in meteoric water across the Nepal Himalaya. Earth and Planetary Science Letters, 183(1-2), 215-229.

Gat, J. R., & Airey, P. L. (2006). Stable water isotopes in the atmosphere/biosphere/lithosphere interface: scaling-up from the local to continental scale, under humid and dry conditions. Global and Planetary Change, 51(1-2), 25-33.

Gat, J. R., & Carmi, I. (1970). Evolution of the isotopic composition of atmospheric waters in the Mediterranean Sea area. Journal of Geophysical Research, 75(15), 3039-3048.

Gile, L. H., Peterson, F. F., & Grossman, R. B. (1966). Morphological and genetic sequences of carbonate accumulation in desert soils. Soil Science, 101(5), 347-360.

Guffanti, M., & Weaver, C. S. (1988). Distribution of late Cenozoic volcanic vents in the Cascade Range: Volcanic arc segmentation and regional tectonic considerations. Journal of Geophysical Research: Solid Earth, 93(B6), 6513-6529.

Hay, R. L. (1962). Soda-rich sanidine of pyroclastic origin from the John Day Formation of Oregon. American Mineralogist: Journal of Earth and Planetary Materials, 47(7-8), 968-971.

Hay, R. L. (1963). Stratigraphy and zeolitic diagenesis of the John Day Formation of Oregon. California: University of California Press.

Kohn, M. J., & Fremd, T. J. (2007). Tectonic controls on isotope compositions and species diversification, John Day Basin, central Oregon. PaleoBios.

Kohn, M. J., & Law, J. M. (2006). Stable isotope chemistry of fossil bone as a new paleoclimate indicator. Geochimica et Cosmochimica Acta, 70(4), 931-946.

Kohn, M. J., Miselis, J. L., & Fremd, T. J. (2002). Oxygen isotope evidence for progressive uplift of the Cascade Range, Oregon. Earth and Planetary Science Letters, 204(1-2), 151-165.

Lander, R. H., & Hay, R. L. (1993). Hydrogeologic control on zeolitic diagenesis of the White River sequence. Geological Society of America Bulletin, 105(3), 361-376.

Lechler, A. R., Huntington, K. W., Breecker, D. O., Sweeney, M. R., & Schauer, A. J. (2018). Loess–paleosol carbonate clumped isotope record of late Pleistocene–Holocene

climate change in the Palouse region, Washington State, USA. Quaternary Research, 90(2), 331-347.

Mack, G. H., Cole, D. R., & Treviño, L. (2000). The distribution and discrimination of shallow, authigenic carbonate in the Pliocene–Pleistocene Palomas Basin, southern Rio Grande rift. Geological Society of America Bulletin, 112(5), 643-656.

McCaffrey, R., King, R. W., Payne, S. J., & Lancaster, M. (2013). Active tectonics of northwestern US inferred from GPS-derived surface velocities. Journal of Geophysical Research: Solid Earth, 118(2), 709-723.

McClaughry, J. D., Ferns, M. L., Streck, M. J., Patridge, K. A., & Gordon, C. L. (2009). Paleogene calderas of central and eastern Oregon: eruptive sources of widespread tuffs in the John Day and Clarno Formations. Volcanoes to vineyards: geologic field trips through the dynamic landscape of the Pacific northwest: Geological Society of America field guide, 15, 407-434.

Methner, K., Fiebig, J., Wacker, U., Umhoefer, P., Chamberlain, C. P., & Mulch, A. (2016). Eocene-Oligocene proto-Cascades topography revealed by clumped (Δ47) and oxygen isotope (δ18O) geochemistry (Chumstick Basin, WA, USA). Tectonics, 35(3), 546-564.

Merlivat, L., & Jouzel, J. (1979). Global climatic interpretation of the deuterium-oxygen 18 relationship for precipitation. Journal of Geophysical Research: Oceans, 84(C8), 5029-5033.

Mulch, A., & Chamberlain, C. P. (2007). Stable isotope paleoaltimetry in orogenic belts–the silicate record in surface and crustal geological archives. Reviews in Mineralogy and Geochemistry, 66(1), 89-118.

Nolan, G. S., & Bindeman, I. N. (2013). Experimental investigation of rates and mechanisms of isotope exchange (O, H) between volcanic ash and isotopically-labeled water. Geochimica et Cosmochimica Acta, 111, 5-27.

O'Neil, J. R., Clayton, R. N., & Mayeda, T. K. (1969). Oxygen isotope fractionation in divalent metal carbonates. The Journal of Chemical Physics, 51(12), 5547-5558.

Pesek, M. E., Perez, N. D., Meigs, A., Rowden, C. C., & Giles, S. M. (2020). Exhumation Timing in the Oregon Cascade Range Decoupled From Deformation, Magmatic, and Climate Patterns. Tectonics, 39(9), e2020TC8.00607

Priest, G. R. (1990). Volcanic and tectonic evolution of the Cascade volcanic arc, central Oregon. Journal of Geophysical Research: Solid Earth, 95(B12), 19583-19599.

Prothero, D. R., Draus, E., & Foss, S. E. (2006). Magnetic stratigraphy of the lower portion of the middle Miocene Mascall Formation, central Oregon. PaleoBios, 26(1), 37-42.

Quade, J., Garzione, C., & Eiler, J. (2007). Paleoelevation reconstruction using pedogenic carbonates. Reviews in Mineralogy and Geochemistry, 66(1), 53-87.

Reidel, S. P., Camp, V. E., Tolan, T. L., & Martin, B. S. (2013). The Columbia River flood basalt province: Stratigraphy, areal extent, volume, and physical volcanology. The Columbia River flood basalt province: Geological Society of America Special Paper, 497, 1-43.

Reiners, P. W., Ehlers, T. A., Garver, J. I., Mitchell, S. G., Montgomery, D. R., Vance, J. A., & Nicolescu, S. (2002). Late Miocene exhumation and uplift of the Washington Cascade Range. Geology, 30(9), 767-770.

Retallack, G. J., Bestland, E. A., & Fremd, T. J. (Eds.). (1999). Eocene and Oligocene paleosols of central Oregon (Vol. 344). Geological Society of America.

Retallack, G. J. (2004). Late Oligocene bunch grassland and early Miocene sod grassland paleosols from central Oregon, USA. Palaeogeography, Palaeoclimatology, Palaeoecology, 207(3-4), 203-237.

Robinson, P. T., Brem, G. F., & McKee, E. H. (1984). John Day Formation of Oregon: a distal record of early Cascade volcanism. Geology, 12(4), 229-232.

Robinson, P. T., Walker, G. W., & McKee, E. H. (1990). Eocene (?), Oligocene, and lower Miocene rocks of the Blue Mountains region. Geology of the Blue Mountains region of Oregon, Idaho, and Washington: Cenozoic geology of the Blue Mountains region. US Geological Survey Professional Paper, 1437, 29-62.

Rohrmann, A., Sachse, D., Mulch, A., Pingel, H., Tofelde, S., Alonso, R. N., & Strecker, M. R. (2016). Miocene orographic uplift forces rapid hydrological change in the southern central Andes. Scientific Reports, 6, 35678.

Rowley, D. B., & Garzione, C. N. (2007). Stable isotope-based paleoaltimetry. Annual. Review Earth and Planetary Science, 35, 463-508.

Ross, C. S., & Smith, R. L. (1955). Water and other volatiles in volcanic glasses. American Mineralogist: Journal of Earth and Planetary Materials, 40(11-12), 1071-1089.

Savin, S. M. (1982). Stable isotopes in climatic reconstructions. In Climate and Earth History (pp. 164-171). Natl. Acad. Press Washington, DC.

Saylor, J. E., & Horton, B. K. (2014). Nonuniform surface uplift of the Andean plateau revealed by deuterium isotopes in Miocene volcanic glass from southern Peru. Earth and Planetary Science Letters, 387, 120-131.

Scanlon, D. P. (2019). The Spatial and Temporal Evolution of the Portland and Tualatin Basins, Oregon, USA [Master's Thesis]. [Portland, Oregon]: Portland State University

Seligman, A. N., Bindeman, I. N., Watkins, J. M., & Ross, A. M. (2016). Water in volcanic glass: From volcanic degassing to secondary hydration. Geochimica et Cosmochimica Acta, 191, 216-238.

Sherrod, D. R., & Smith, J. G. (2000). Geologic map of upper Eocene to Holocene volcanic and related rocks of the Cascade Range, Oregon (p. 17). Washington, DC: US Geological Survey.

Smith, G. A., Snee, L. W., & Taylor, E. M. (1987). Stratigraphic, sedimentologic, and petrologic record of late Miocene subsidence of the central Oregon High Cascades. Geology, 15(5), 389-392.

Snavely JR, P. D., MacLeod, N. S., & Wagner, H. C. (1973). Miocene tholeiitic basalts of coastal Oregon and Washington and their relations to coeval basalts of the Columbia Plateau. Geological Society of America Bulletin, 84(2), 387-424.

Stevenson, B. (1997). The Stable Carbon Isotope Composition of Paleosols in Pleistocene Palouse Loess (Doctoral dissertation, Ph. D. Dissertation, Soil and Crop Sciences Department, Colorado State University, Fort Collins, CO).

Streck, M. J., & Grunder, A. L. (1995). Crystallization and welding variations in a widespread ignimbrite sheet; the Rattlesnake Tuff, eastern Oregon, USA. Bulletin of Volcanology, 57(3), 151-169.

Tabor, R. W., Frizzell Jr, V. A., Vance, J. A., & Naeser, C. W. (1984). Ages and stratigraphy of lower and middle Tertiary sedimentary and volcanic rocks of the central Cascades, Washington: Application to the tectonic history of the Straight Creek fault. Geological Society of America Bulletin, 95(1), 26-44.

Takeuchi, A., & Larson, P. B. (2005). Oxygen isotope evidence for the late Cenozoic development of an orographic rain shadow in eastern Washington, USA. Geology, 33(4), 313-316.

Takeuchi, A., Hren, M. T., Smith, S. V., Chamberlain, C. P., & Larson, P. B. (2010). Pedogenic carbonate carbon isotopic constraints on paleoprecipitation: Evolution of desert in the Pacific Northwest, USA, in response to topographic development of the Cascade Range. Chemical Geology, 277(3-4), 323-335.

Taylor, S. B., Johnson, S. Y., Fraser, G. T., & Roberts, J. W. (1988). Sedimentation and tectonics of the lower and middle Eocene Swauk Formation in eastern Swauk Basin, central Cascades, central Washington. Canadian Journal of Earth Sciences, 25(7), 1020-1036.

Uemura, R., Matsui, Y., Yoshimura, K., Motoyama, H., & Yoshida, N. (2008). Evidence of deuterium excess in water vapor as an indicator of ocean surface conditions. Journal of Geophysical Research: Atmospheres, 113(D19).

Verplanck, E. P., & Duncan, R. A. (1987). Temporal variations in plate convergence and eruption rates in the Western Cascades, Oregon. Tectonics, 6(2), 197-209.

Wells, R. E., & McCaffrey, R. (2013). Steady rotation of the Cascade arc. Geology, 41(9), 1027-1030.

Wells, R., Bukry, D., Friedman, R., Pyle, D., Duncan, R., Haeussler, P., & Wooden, J. (2014). Geologic history of Siletzia, a large igneous province in the Oregon and Washington Coast Range: Correlation to the geomagnetic polarity time scale and implications for a long-lived Yellowstone hotspot. Geosphere, 10(4), 692-719.

Wells, R. E., Weaver, C. S., & Blakely, R. J. (1998). Fore-arc migration in Cascadia and its neotectonic significance. Geology, 26(8), 759-762.

Wells, R. E., & McCaffrey, R. (2013). Steady rotation of the Cascade arc. Geology, 41(9), 1027-1030.

Wolfe, J. A. (1994). Tertiary climatic changes at middle latitudes of western North America. Palaeogeography, Palaeoclimatology, Palaeoecology, 108(3-4), 195-205.

Yeh, H. W., & Savin, S. M. (1977). Mechanism of burial metamorphism of argillaceous sediments: 3. O-isotope evidence. Geological Society of America Bulletin, 88(9), 1321-1330.

Zachos, J., Pagani, M., Sloan, L., Thomas, E., & Billups, K. (2001). Trends, rhythms, and aberrations in global climate 65 Ma to present. science, 292(5517), 686-693.

Appendix A- Description of Supplementary Tables:

Table S1: Compilation of stable isotope, location, and source data for all samples considered in this paper.xlsx 332 KB. May be viewed using Microsoft Excel.

Table S2: Modern water data for the Pacific Northwest.xlsx 52KB. May be viewed using Microsoft Excel.

Appendix B-Sample Descriptions and Locations

Volcanic Glass

COS01 and COS02 are Tuff of Smith Rock samples and the location is the Haystack Reservoir North Fishing Dock from McClaughry et al., (2009) Stop #5. The Tuff of Smith Rock is an ash-flow tuff which is correlative to the Picture Gorge Ignimbrite Member G. COS01 is taken from an outcrop on the north side of the parking lot. The sample is quartz rich, red, and massive. COS02 is taken from an outcrop exposed alongside a river flowing through the reservoir northeast of the parking area (Fig B-1).

Both outcrops feature tabular ~10 cm thick beds which are consistent thickness laterally (tabular) and have poor sorting. The GPS location is 44.496389, -121.155861 with an elevation of 863m.

Figure B-1. Picture of outcrop from which COS02 is taken. Photo is looking west ~10m northeast of Haystack Reservoir North Fishing Area Parking Lot.

COS03 is Picture Gorge Ignimbrite float taken from atop the Carroll Rim Viewpoint in John Day National Monument (Fig B-2). The Picture Gorge Ignimbrite is a rhyolitic ash flow tuff. The sample is tan-brown with some red oxidation streaks as well as some blue mottling on the exterior. I am confident that this sample is recently exposed

due to the relatively narrow and high ridge this sample was collected from. Its GPS location is approximately 44.656, -120.27.

Figure B-2. Picture of where COS03 was sampled from. Photo is looking east atop the Carroll Rim in John Day National Monument.

COS05 is the Sanidine Tuff of Hay (1962) sampled from the Lower Turtle Cove Member of Retallack et al. (1999), section 10B. The Sanidine Tuff is a rhyolitic ash flow. Beds are very well sorted, tabular, and ~1m thick. The sample is welded and very ash rich. Its location is 44.66, -120.27.

Figure B-3. Picture of outcrop where COS05 is sampled from. Picture is looking east into the west side of Carroll Rim.

Figure B-4. Outcrop scale picture of where COS05 is sampled from. Picture is looking west from the west side of the Carroll Rim.

COS10 is Picture Gorge Ignimbrite sampled from the top of a Turtle Cove cliff a quarter mile north of the Foree Camping Area in John Day National Monument. The outcrop contains interbedded, resistant ash flows. The sample is very welded, with a GPS location of 44.66, -119.64.

COS18 is from John Day Formation Member A of Robinson et al. (1984). Member A is a regionally extensive ash-flow tuff. The sample was collected from the Ignimbrite Rim by the Hancock Field Station in the Clarno area of the John Day National Monument (Fig B-5). The sample is poorly sorted, breccia-like in texture, and red. The outcrop is very densely welded. Its location is 44.93, -120.42.

Figure B-5. Picture of outcrop where COS18 is sampled from. Picture is looking north from Ignimbrite Rim

Carbonates

COS04 is from the Turtle Cove Member sampled while descending the west side of Carroll Rim in John Day National Monument. The sample is conglomeritic, tan-white, and moderately friable. White nodules ~2mm in diameter are abundant and more reactive to HCl compared to the groundmass. The sample is classified as Yapas pedotype of Retallack (1999). Its location is 44.66, -120.25.

Figure B-6 Picture of the outcrop where COS04 is sampled from. Picture is looking east from the west side of the Carroll Rim.

COS06 is from the Turtle Cove Member and sampled ~5m below COS05. The sample is a green, medium-grained sandstone of the Xaxus pedotype (Retallack et al., 1999). The sample is weakly calcareous, with ~2mm diameter nodules that are more reactive with HCl. Its location is 44.66, -120.27.

COS07 is from the Kimberly Member sampled ~1.5km southwest of the junction of Highway 26 and Highway 19, just outside of the John Day National Monument. The outcrop contains visible paleosol horizons and root casts. The sample is a fine-grained sandstone, white-yellow and very friable. It is highly reactive with HCl, which penetrates very quickly through the sample. Possible cicada burrows are present throughout the outcrop. Its location is 44.51, -119.66.

Figure B-7. Outcrop where COS07 was sampled from. Picture is looking south into the outcrop off of Highway 26 ~1km southwest of the junction of Highway 26 and Highway 19. Areas where the rock protrude out more are slumped B horizons.

COS11 and COS12 are large (8cm diameter) nodules sampled off a cliff a quarter mile north of the Foree Picnic Area in the John Day National Monument. The outcrop is mostly pale-green to grey sandstone with ~1mm white clasts. The groundmass is weakly calcareous. Nodules are found in relatively thick layers about ~1m apart. Sampled nodules are tan-red on the outside and tan-gray on the inside. The outer red shell is slightly reactive to HCl and the interior is highly reactive. Its location is 44.66, -119.64.

Figure B-8. Picture of the outcrop where COS11 and COS12 are sampled from. Picture is taken looking north into a cliff near Foree.

COS13, COS14 and COS15 are Kimberly Member samples taken from cliffs on the north side of the road towards Monument, Oregon, 1km northeast of Kimberly, Oregon, along Long Creek Highway. These samples are from the Kimberly Member of Retallack (2004). This outcrop features repeating paleosol sequences with notable horizons. The interpreted B and Bk horizons are much thicker than the A horizons and feature tan nodules, which I sampled. These nodules are highly calcareous. The groundmass is tan-yellow siltstone and weakly calcareous. Some root fossils are also visible in the outcrop. COS15 was the lowest in stratigraphy while COS13 was ~3 meters

above COS15, and COS14 was another ~3m above COS13. Their location is 44.77, -119.63.

Figure B-9. Picture of outcrop where COS14 is sampled from, which is above where COS13 and COS15 are sampled from. Picture is looking east from a roadcut on the north side of Long Creek Highway ~1km northeast of Kimberly.

Figure B-10. Picture of outcrop where COS13 is sampled from, which is above where COS15 is sampled from and below COS14. Picture is looking south from roadcut on the northside of Long Creek Highway ~1km northeast of Kimberly.

Sample JDRL2 is from the Big Basin Member and taken from a cliff 600m northeast of Cant Ranch in John Day National Monument. The sample is a highly friable, red-purple claystone that is moderately calcareous. Its location is 44.56, -119.64.

Figure B-11. Picture of outcrop where JDRL2 is sampled from. Picture is looking north, into the outcrop which is 600m northeast of Cant Ranch.

JDRL4 is from the Turtle Cove Member sampled at the base of a cliff ~500m due east of Cant Ranch in John Day National Monument. The outcrop alternates between green and grey sandstones which are weakly calcareous and mostly classified as the Xaxus pedotype (Retallack et al., 1999). The sample is a 5cm diameter red-tan nodule, which is highly calcareous. Its location is 44.56, -119.64.

Figure B-12. Picture of outcrop where JDRL4 was sampled from. The red rock is a carbonate nodule, which was sampled over the grey groundmass. Picture is looking north from outcrop which is 500m due east of Cant Ranch

Samples JDRL5, JDRL6, JDRL7 and JDRL8 are classified as the Yapas pedotype (Retallack et al., 1999) and were collected in badlands behind the house of Nina Hopper 3km east of Spray. This is the Balm Creek Section of the Kimberly Member of Retallack (2004). Samples are yellow-tan nodules of ~2-5cm diameter. The outcrop is mostly yellow-tan siltstone with abundant plant fossils and root casts. Paleosol horizons are visible in places with B horizons often demonstrating slumping. These samples were collected moving up stratigraphy with 1.5-3 meters between each. Their location is 44.835228, -119.743167.

Figure B-13 Picture of outcrop from which JDRL5, JDRL6, JDRL7 and JDRL8 are sampled from. Rounded features are carbonate nodules, which were sampled over the groundmass. Nodules are highly calcareous and vary in size from 2-5cm. Picture is looking northwest into the outcrop in the badlands 3km east of Spray.

Samples Reanalyzed from Carlson (2018)

CVG013 of Carlson (2018) is a Tuff of Dale sample. This is a rhyolitic ash flow sampled by the North Fork of the John Day River. The sample is light, grey, vitric, and partially welded.

CVG036 is a Picture Gorge Ignimbrite sample. This is a rhyolitic ash flow tuff of the John Day Formation. The sample is grey, vitric, and welded. Carlson (2018) analyzed this sample, but interpreted it as magmatically influenced due to a low wt. % H_2O.

CVG034 and CVG033 are both of the Mascall Formation, which is mostly ash-fall tuffs. CVG034 is the Kangaroo tuff, an off white-yellow ash that is welded and vitric. CVG033 is the Mascall Tuff, which is white, grey and vitric. Carlson (2018) did not analyze these samples, as much of them dissolved during HF rinsing, suggesting devitrification.

CVG037 is a John Day Formation Member A sample. This sample is white, very welded, and described as vitric. Carlson (2018) did not analyze this sample as it appeared highly altered under petrographic microscope. I analyzed it alongside a newly collected John Day Formation Member A sample after further HF rinsing, as the sample appeared to be approaching 99% purity.

Appendix C- Additional Data

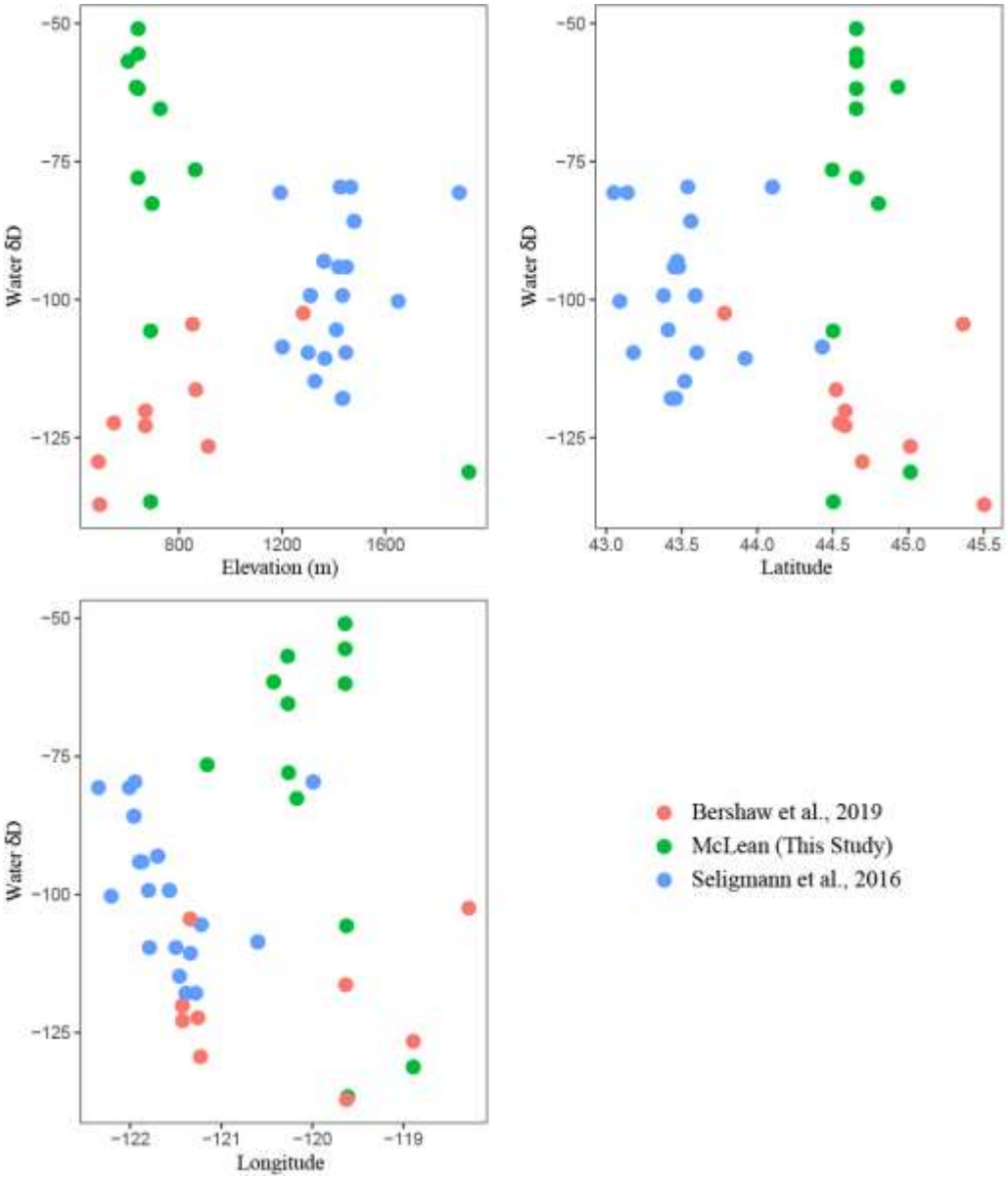

Figure C-1. Plots showing the relationship between water δD of Oregon volcanic glass and elevation (top left), latitude (top right), and longitude (bottom left). There is no significant correlation between δD and any of the three variables.

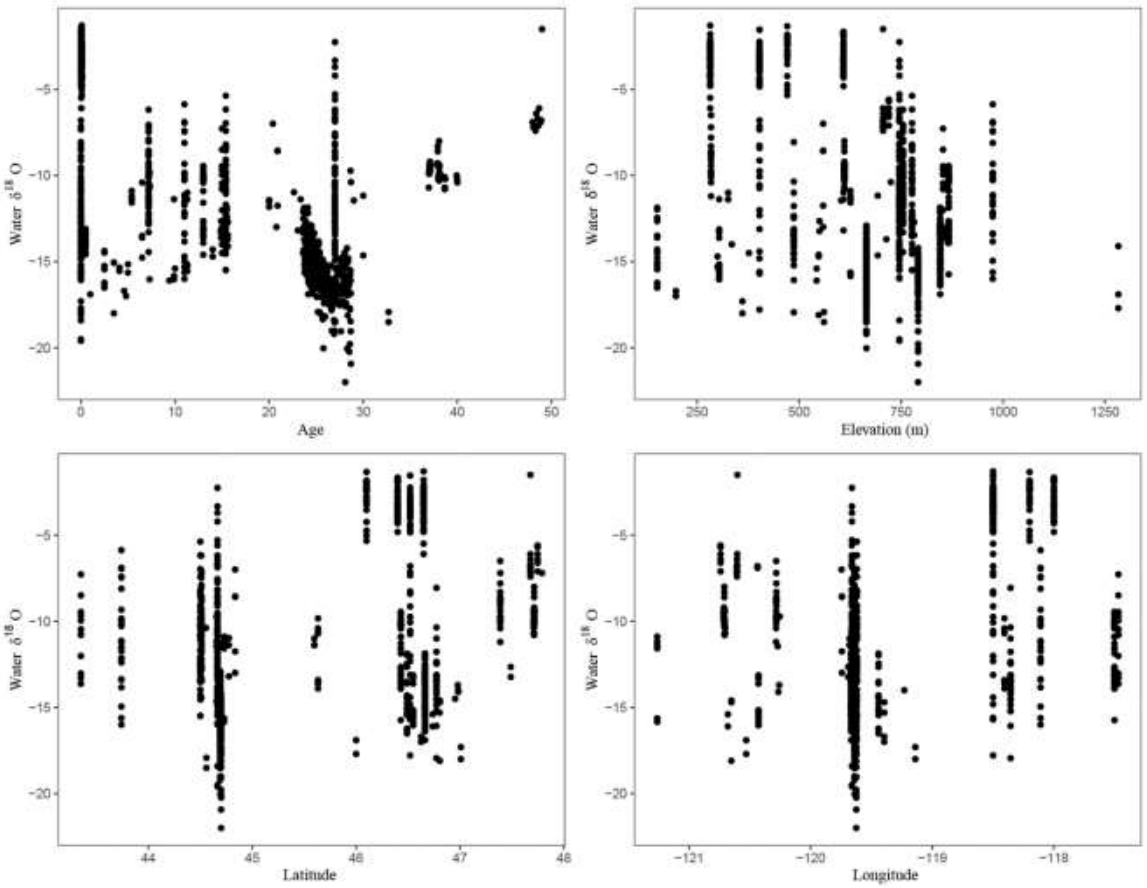

Figure C-2. Plots showing the relationship between water $\delta^{18}O$ of oxygen proxies from the Pacific Northwest and age (top left), elevation (top right), latitude (bottom left) and longitude (bottom right). There is no significant correlation between $\delta^{18}O$ and any of the four variables.

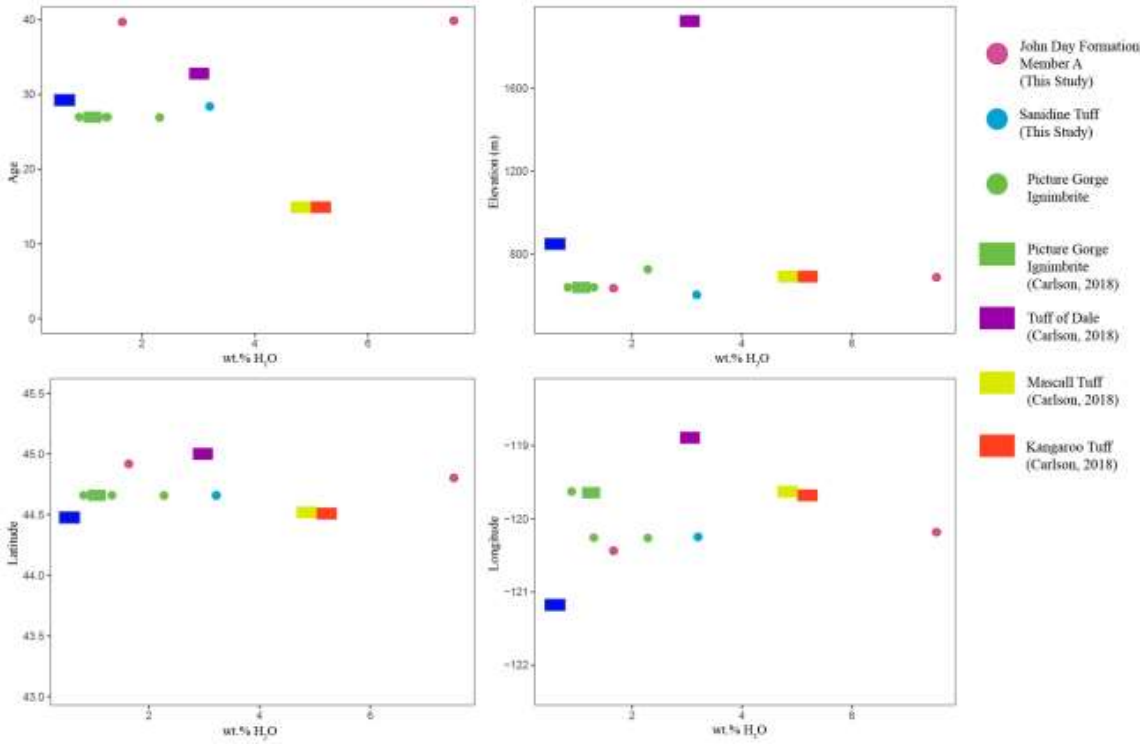

Figure C-3. Plots showing the relationship between wt. % H_2O in Oregon volcanic glass samples analyzed in this study and age (top left), elevation (top right), latitude (bottom left), and longitude (bottom right). Squares indicate samples that were collected by Carlson (2018) and analyzed in this study. There is no significant correlation between wt. % H_2O and any of the four variables.